Quantum Chemical Studies on Detail Mechanism of Nitrosylation of NAMI-A-HSA Adduct

ARTICLE · JULY 2015

DOI: 10.1021/acs.jpcb.5b05071 · Source: PubMed

THE JOURNAL OF PHYSICAL CHEMISTRY B

Article

pubs.acs.org/JPCB

Quantum Chemical Studies on Detail Mechanism of Nitrosylation of NAMI-A-HSA Adduct

Dharitri Das and Paritosh Mondal*

Department of Chemistry, Assam University, Silchar 788011, Assam, India

Supporting Information

ABSTRACT: Hydrolysis of NAMI-A in NAMI-A-HSA (HSA = human serum albumin) and nitrosylation of hydrolyzed NAMI-A-HSA adduct have been studied in detail using density functional theory method. It has been observed that the chloride exchange reaction with water in the NAMI-A-HSA adduct follows an interchange dissociative mechanism passing through an unstable heptacoordinated activated complex. The computed free energy of activation (ΔG) and rate constant (k) for the hydrolysis process in aqueous medium are observed to be 24.85 kcal mol^{-1} and 3.81 × 10^{-6} s^{-1}, respectively. Nitrosylation of hydrolyzed NAMI-A-HSA adduct with nitric oxide is found to be thermodynamically more favorable with the incorporation of solvent effect and provides a detailed understanding related to the antimetastatic activity of the NAMI-A drug. This investigation shows that nitric oxide coordinates linearly to NAMI-A-HSA adduct leading to the reduction of ruthenium(III) to more active ruthenium(II), with the reduction potential of −2.32 V. Negative relative solvation and relative binding free energies suggest that the hydrolysis and nitrosylation reactions are found to be thermodynamically favorable and faster. Our computed results provide a detailed thermodynamics and kinetics which may be highly beneficial for understanding antimetastatic activity as well as the nitric oxide scavenging ability of NAMI-A.

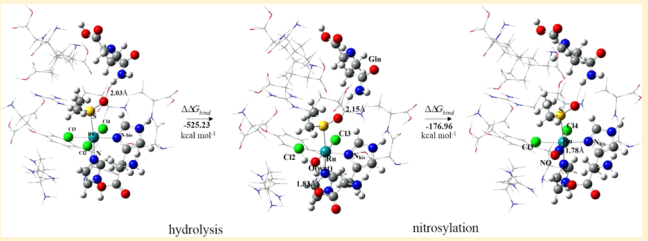

INTRODUCTION

Over the past 3 decades, anticancer chemotherapies focused mainly on cisplatin derivatives. Even then they have profound side effects in most cancer treatments along with their inactivity toward some cancers.[1] Thus, searches for new drugs with improved anticancer activity have led to the discovery of many nonplatinum metal based drugs. Among these, ruthenium complexes appear to be most promising, having interesting anticancer properties *in vivo* and lesser cytotoxic effect.[2] Ruthenium possesses three main properties that make it well suited for medicinal application which are multiple accessible oxidation states, ligand exchange kinetics, and the ability to mimic iron in binding to certain biomolecules.[3] Ruthenium is a particular metal which is characterized by the fact that oxidation states ruthenium(II) and ruthenium(III) are easily accessible under physiologically relevant conditions and hence make this metal unique among the platinum group.[4] The biological activity of these ruthenium complexes were recognized for the first time in the 1950s[5] and their anticancer activity in the 1960s.[6] Among the wide group of synthesized ruthenium complexes, two ruthenium agents, NAMI-A and KP1019, are currently in human clinical trials.[7,8] KP1019 is active against colon cancer[9] while NAMI-A has been found to be active in inhibiting the formation and growth oflung, mammary, and B16F10 melanoma metastases.[10−12] However, NAMI-A exhibits lower activity toward primary tumors. The mode of action of these antimetastatic drugs is thought to be different from that of the platinum drugs.[13] Numerous *in vivo* and *in vitro* studies suggest various modes of action of NAMI-A which include the following: blocking the development of the cell cycle at the G2M premitotic phase, apoptosis in endothelial cells, and interaction with actin-type proteins on the extracellular matrix around tumor vasculature, leading to inhibition of invasiveness.[14,15] Aquation and reduction processes are supposed to be the two key activation steps of NAMI-A before it reaches its intracellular target. Aquation of NAMI-A occurs in the bloodstream[16] which leads to the exchange of one or more chloride ligands with water molecules, producing more reactive species. NAMI-A with two chloro and two aqua ligands is found to be significant for its biological activity.[17] On the other hand, considering the redox environment such as ascorbic acid, cysteine, and so on in the bloodstream or glutathione in the cell, reduction from ruthenium(III) to ruthenium(II) can be

Scheme 1. Thermodynamic Cycles for Calculating the Relative Solvation Free Energy and Relative Binding Free Energy

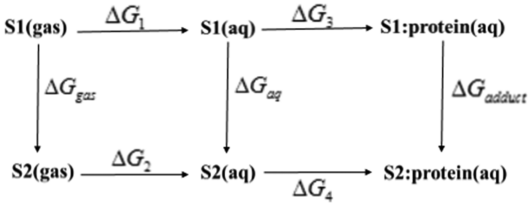

Received: May 28, 2015
Revised: July 7, 2015
Published: July 7, 2015

DOI: 10.1021/acs.jpcb.5b05071
J. Phys. Chem. B 2015, 119, 10456−10465

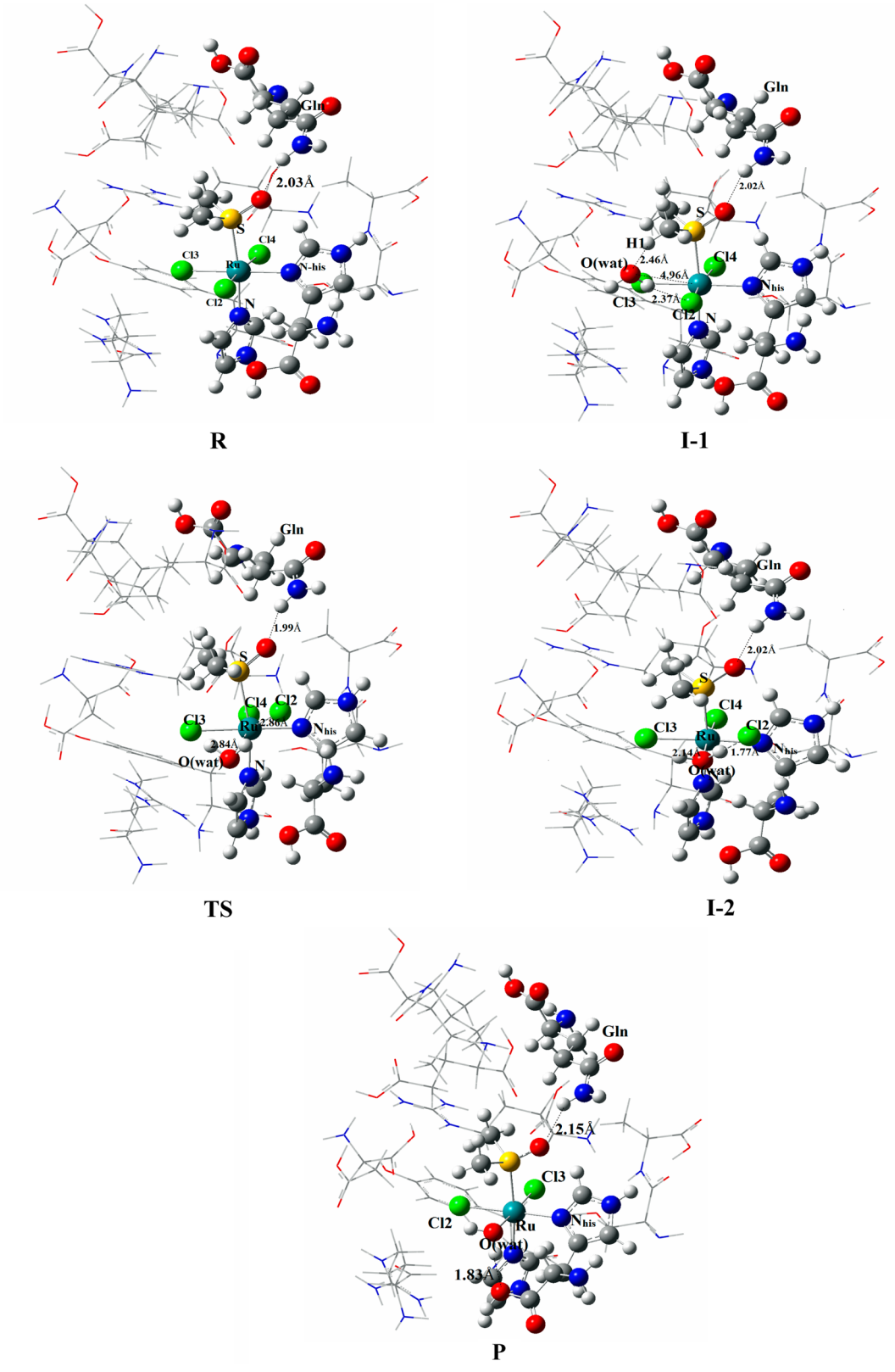

Figure 1. Optimized structures for the species involved in hydrolysis reaction of NAMI-A-HSA adduct calculated at the B3LYP/(LanL2DZ+6-31G(d,p)) level.

expected.[18] NAMI-A can be transported into cancer cells by binding to serum transferrin, a glycoprotein that delivers iron in these cells through the receptor-mediated endocytosis.[19] In blood plasma, only 30% of transferrin remains in the holo form (coordinating to Fe^{2+} ions) and the remaining 70% of transferrin is found in the apo form which can be used for binding various ions at the same binding sites as iron.[20] Because ruthenium is in the same group as iron, they have many similar characteristics

DOI: 10.1021/acs.jpcb.5b05071
J. Phys. Chem. B 2015, 119, 10456−10465

and, hence, ruthenium ion of NAMI-A can also bind transferrin like iron ion.[21] Cancer cells have many transferrin receptors available because of their increased demand for iron, and therefore the delivery of NAMI-A can be enhanced.[16] In the tumor site, NAMI-A interacts with cancer cells, resulting in inhibition of growth and causing apoptosis. However, these proposed mechanisms are just based on hypothesis, and the actual biological mechanism of NAMI-A is yet to be known. Recent investigations proposed that the interference of NAMI-A with nitric oxide may be one of the possible routes for its antimetastatic activity[22,23] because nitric oxide is involved in contributing to the progression of many tumors and has the ability to interact with metal complexes.[24]

Nitric oxide (NO), produced by a number of nitric oxide synthase (NOS) enzymes from L-arginine in the body,[25] is an important signaling molecule involved in the regulation of different physiological processes such as neural transmission, regulation of cardiovascular function, apoptosis, and immune defense in mammals.[26] On the other hand, being a free radical, nitric oxide is highly toxic to the cells. NO exhibits an important role in maintaining the vasodilatory tone of tumors by regulating tumor blood flow[27] and is closely linked to the growth and progression of several human tumors.[28−30] It also acts as an active mediator for the tumor angiogenesis.[31,32] Systematic inhibition of nitric oxide synthase (NOS) or inactivation of free NO in tumors through the availability of drug molecules has been demonstrated as a new alternative therapeutic approach toward inhibiting tumor angiogenesis.[33] NAMI-A is reported to have an angiogenesis inhibitory activity.[34,35] Increasing evidence in the literature has shown that NAMI-A, KP1339 (Na[*trans*-$RuCl_4(Ind)_2$], Ind = indazole),[7,36,37] and Ru(EDTA) complexes capable of inhibiting NO-dependent angiogenesis by capturing NO *in vivo* and *in vitro* without affecting the intracellular mechanism involved in proliferation.[38,39] NO interacts with NAMI-A and other ruthenium(III) complexes in a linear fashion to give ruthenium nitrosyl complexes which are formally described as $[Ru^{II}-NO^{+}]$.[15] Change in the oxidation state of the ruthenium(III) occurring upon NO binding is characterized by a weak absorption band at around 500 nm and is substantially different from parent ruthenium(III) complexes characterized by relatively strong ligand-to-metal charge transfer bands.[40] Along with its antimetastatic and antiangiogenesis activities, ruthenium(III) complexes have also been investigated as nitric oxide scavengers.[41,42] The NO scavengers will be effective if they will meet the criteria such as fast NO reaction kinetics, activity and stability of *in vitro* and *in vivo* biological systems, low toxicity, and rapid clearance from the organism.[39]

Until now, there have been a number of experimental reports on the nitrosylation reaction of ruthenium-based drugs that have been done, but to the best of our knowledge only a few computational studies have been performed at the molecular level. The aim of our present study is to investigate the NO scavenging capability of the clinically established ruthenium(III) complex, at the molecular level. We have studied the interaction mechanism of NAMI-A-HSA (HSA = human serum albumin) with NO, because NAMI-A binds to the plasma proteins after intravenous administration. The NAMI-A-HSA adduct has been taken from our previous studies on ruthenium(III) complex−protein interaction.[43] The structure of the NAMI-A-HSA adduct is obtained from the molecular docking simulation whose stability is further confirmed from ONIOM calculation. Hydrolysis of NAMI-A-HSA adduct has been performed prior to reaction with NO in which one of the Cl^- ligands is substituted with a water ligand. Water being a labile substituent in the NAMI-A-HSA adduct can easily exchange with various ligands.

Table 1. Optimized Geometric Parameters (Bond Lengths, Å; Bond Angles, deg) of All of the Stationary Points in Chloride Exchange Reaction of NAMI-A-HSA Adduct with Water at the Level of B3LYP/(LANL2DZ+6-31G(d,p) in Gas Phase

param	R	I-1	TS	I-2	P
Ru—N_{his}	2.18	2.18	2.16	2.13	2.15
Ru—Cl2	2.42	2.42	2.86	4.14	
Ru—Cl3	2.38	2.38	2.44	2.39	2.38
Ru—Cl4	2.40	2.41	2.38	2.36	2.33
Ru—S	2.43	2.44	2.51	2.49	2.45
Ru—N	2.11	2.11	2.13	2.10	2.12
Ru—O(wat)		4.96	2.84	2.14	2.23
H1—O(wat)		2.46			
Cl2—H(wat)		2.37	2.07	1.77	
O(his)—H(wat)					1.83
DMSO—H_{Gln}	2.03	2.02	1.99	2.02	2.15
N1—Ru—S1	172.8	172.5	166.9	171.7	173.6
N_{his}—Ru—Cl2	88.1	87.0	70.3	60.5	
Cl2—Ru—Cl3	92.8	93.1	115.2	97.0	
Cl3—Ru—Cl4	93.4	93.8	91.0		96.4
Cl4—Ru—N_{his}	85.7	86.1	83.9	89.9	88.4
O(wat)—Ru—Cl3			70.6	85.7	81.9
O(wat)—Ru—N_{his}				87.5	91.6

COMPUTATIONAL DETAILS

Hydrolysis and nitrosylation reaction mechanisms of NAMI-A-HSA adduct have been carried out using the density functional theory, employing the Gaussian 09 program package.[44] The gas phase optimization of reactants, products, and transition states without imposing any symmetry constraint has been done using unresrticted B3LYP[45] exchange-correlation functional with 6-31G(d,p)[46] and LANL2DZ[47] basis sets. The effective core potential basis set LANL2DZ for ruthenium atom and the 6-31G(d, p) basis set for all other atoms are used. A vibrational analysis has been performed at the same level of theory, to ensure that optimized structures are minima or transition states and to estimate zero-point vibrational energies and thermal and entropic corrections. The transition states are also confirmed by intrinsic reaction coordinate (IRC) calculations.[48,49] In order to obtain energies for the reaction surfaces, single-point energies are calculated on optimized geometries using the higher basis sets of LanL2DZ (on Ru atom), 6-311+G(d, p) (on H, C, N, and O atoms), and 6-311+G(3d)(on Cl and S atoms) *in vacuo*.[50,51] Single-point energies are also evaluated using implicit solvation model CPCM.[52]

Free energies, enthalpies, and solvation free energies are computed by using the following equations:[53]

$$G_{solv} = G_{solvent} - G_{gas}$$

$$H(aq) = E_{tot/ZPE}(g) + G_{solv} + H_{therm}(g)$$

$$G(aq) = H(aq) - TS$$

where G_{solv} is the solvation free energy, $G_{solvent}$ is the Gibbs free energy in solvent medium, and G_{gas} is the Gibbs free energy in gas phase. $H(aq)$ is the enthalpy,$G(aq)$ is the Gibbs free energy in aqueous medium, $H_{therm}(g)$ is the thermal correction to enthalpy, and S is the entropy in the gas phase. These values are obtained through single-point energy calculation at the level of

DOI: 10.1021/acs.jpcb.5b05071
J. Phys. Chem. B 2015, 119, 10456−10465

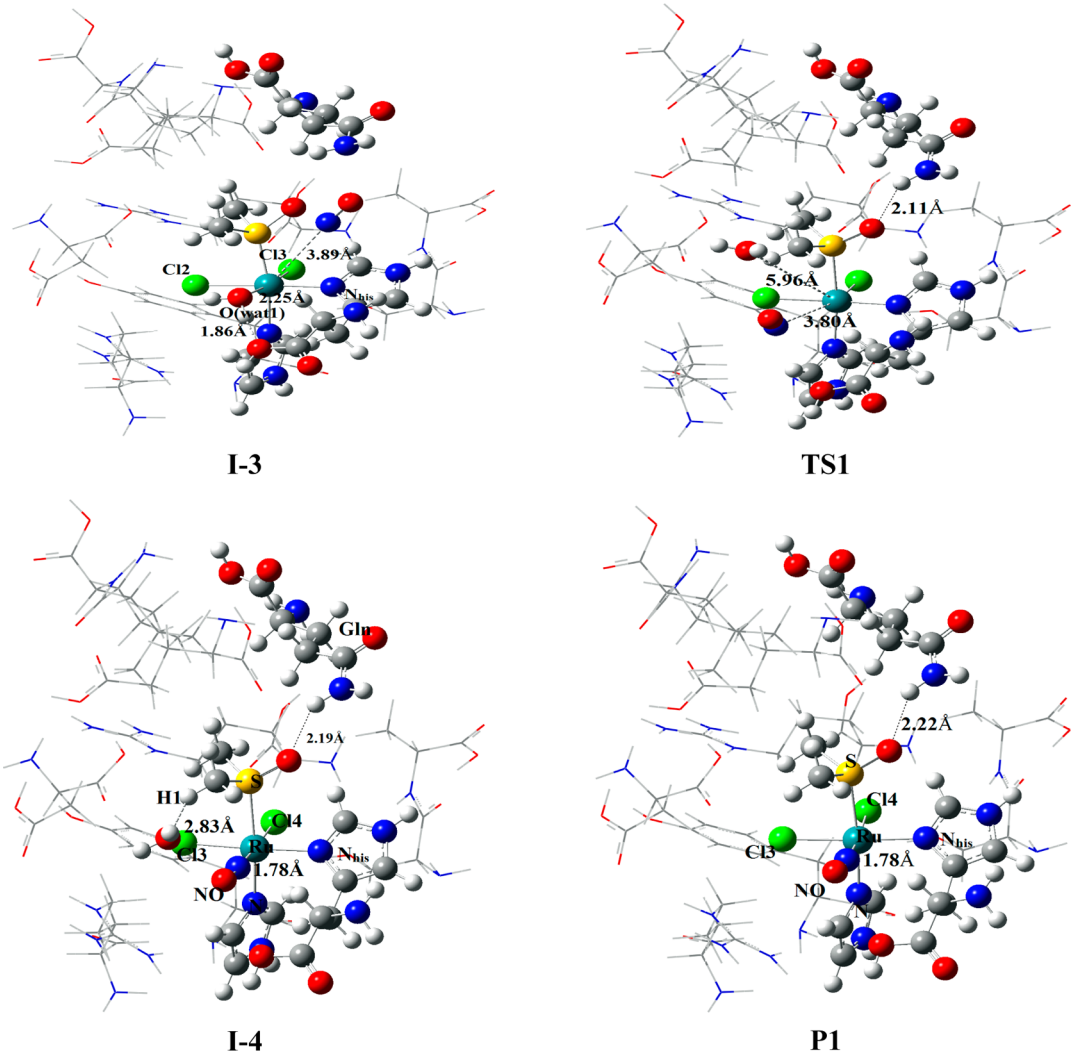

Figure 2. Optimized structures for the species involved in nitrosylation reaction of hydrolyzed NAMI-A-HSA adduct calculated at the B3LYP/(LanL2DZ+6-31G(d,p)) level.

UB3LYP/(LanL2DZ+6-311+G(d, p)+6-311+G(3d)) at 298.15 K on the optimized geometries.

Activation free energy (free energy difference between the transition state and original state) is used to calculate the rate constant for all of the substitution reactions via transition state theory formalism[54] proposed by Eyring as

$$k(T) = \frac{K_B T}{h} e^{-\Delta G^{\ddagger}/RT}$$

where K_B is the Boltzmann constant, T is the absolute temperature, and $\Delta G^{\ddagger}$ is the activation free energy.

Reduction potentials (E_m) at standard conditions are obtained from the following equation:

$$E_m = \Delta G/nF$$

F is the Faraday constant (F = 96485 C/mol), E_m is the reduction potential, and n is the number of electrons that take part in the redox reaction.

THERMODYNAMIC CYCLIC PERTURBATION METHOD

Mc Cammon and co-workers around the 1980s had applied the concept of perturbation theory for the first time to computationally measure ligand-binding affinities in terms of free energy.[55] The basic approach of this perturbation method is to compute free energy changes via nonphysical transformation, which involves alteration of one ligand to a structurally different ligand. This procedure has been currently employed for obtaining relative binding free energies ($\Delta\Delta G_{bind}$). A schematic representation of a thermodynamic cyclic perturbation for protein−ligand interaction is shown in Scheme 1.

For thermodynamic cycles that relate the difference in free energy between two ligands S1 and S2 in two media gas and solvent, then the double free energy difference will correspond to the relative solvation free energy change of S2 with respect to S1 shown in Scheme 1 and represented by the following equation:

$$\Delta\Delta G_{solv} = \Delta G_2 - \Delta G_1 = \Delta G_{aq} - \Delta G_{gas}$$

The double free energy difference will correspond to the relative binding free energy of ligand S2 with respect to S1 if the two media are solvated protein and pure water. The equation is represented as

$$\Delta\Delta G_{bind} = \Delta G_4 - \Delta G_3 = \Delta G_{adduct} - \Delta G_{aq}$$

DOI: 10.1021/acs.jpcb.5b05071
J. Phys. Chem. B 2015, 119, 10456−10465

RESULTS AND DISCUSSION

Structural Characteristics. *Hydrolysis.* Fully optimized structures of all of the species involved in the hydrolysis of NAMI-A-HSA adduct calculated at the B3LYP/(LANL2DZ+6-31G(d,p)) level are presented in Figure 1, and significant geometrical parameters are listed in Table 1. From Figure 1 and Table 1, it is seen that, in the reactant R, NAMI-A retains its pseudo-octahedral geometry with three equatorial chloro ligands, one equatorial histidyl residue, and two axial ligands, namely, DMSO and imidazole group. The Ru—Cl1, Ru—Cl2, Ru—Cl3, Ru—N_{his} bond distances are found to be 2.42, 2.40, 2.38, and 2.18 Å whereas Ru—N and Ru—S bond lengths are calculated to be 2.11 and 2.43 Å, respectively. The bond angles Cl1—Ru—N_{His} and Cl2—Ru—N_{His} are observed to be 85.7° and 88.1°, respectively. Observed deviation of the bond angle from 90° reveals the hexacoordinated distorted octahedral geometry of R. Table 1 suggests that DFT computed bond distances are found to be slightly longer than the X-ray crystallographic data.[56] These differences in bond distances may be due to the systematic error caused by the computational methods and environment factors.[57] It is also observed that NAMI-A forms a hydrogen bonding between DMSO oxygen atom and one of the hydrogen atoms of glutamine side chain (2.03 Å). The presence of hydrogen bonding gives additional stability to R. The initial geometry of intermediate I-1 is obtained by putting the reactant R and a water molecule at a distance of Ru—O(wat) = 4.06 Å which, on optimization, gives I-1. In I-1, the water molecule approaches the reaction center via the hydrogen bond with the adjacent Cl^- ligand (HOH···Cl) at a distance of about 2.37 Å. Hence, in the product intermediate, I-2, the Ru—O(wat) distance was taken to be 2.78 Å and then optimized. The geometry of product intermediate I-2 is observed to be pseudo-octahedral in which Cl^- ligand is completely exchanged by water ligand and forms a bond with Ru^{3+} ion at a distance of 2.14 Å. Again the leaving Cl^- ligand forms intermolecular hydrogen bonding with a H atom of the coordinated water molecule at a distance of 1.77 Å. Using the optimized geometries of I-1 and I-2, a synchronous transit-guided quasi-Newton approach (QST3) for the transition state was conducted and the structure so obtained is designated as TS. The transition state found for the hydrolysis step of NAMI-A-HSA adduct is confirmed by the presence of an imaginary frequency and has pentagonal bipyramidal arrangement. The Ru—O(wat) bond distance is reduced from 4.96 Å in I-1 to 2.84 Å in TS, while the Ru—Cl2 distance increases from 2.42 to 2.86 Å; hence, it follows an interchange dissociative mechanism. On the other hand, product P attains a pseudo-octahedral configuration, where Cl^- ligand is completely removed from the system and the coordinated water molecule forms a hydrogen bond with O atom of histidyl residue at a distance of 1.83 Å. During this entire hydrolysis path of the NAMI-A-HSA adduct, the ruthenium ion remains in its +3 oxidation state.

Nitrosylation. Figure 2 displays the optimized stationary points for nitrosylation of P (hydrolyzed product of NAMI-A-HSA adduct) with nitric oxide, and the important geometrical parameters are summarized in Table 2. The same procedures were adopted to obtain the geometry of I-3, I-4, TS1, and P1 as mentioned in the hydrolysis of NAMI-A-HSA adduct. In the

Table 2. Optimized Geometric Parameters (Bond Lengths, Å; Bond Angles, deg) of All of the Stationary Points in Water Exchange Reaction of Hydrolyzed NAMI-A-HSA Adduct with Nitric Oxide at the Level of B3LYP/(LANL2DZ+6-31G(d,p) in Gas Phase

param	I-3	TS1	I-4	P1
Ru—N_{his}	2.15	2.12	2.17	2.17
Ru—Cl3	2.47	2.33	2.42	2.42
Ru—Cl4	2.42	2.29	2.37	2.36
Ru—S	2.26	2.46	2.48	2.49
Ru—N	2.11	2.11	2.13	2.12
O(his)—H(wat)	1.86			
Ru—O(wat)	2.25	5.96	5.03	
Ru—N(NO)	3.89	3.80	1.78	1.78
DMSO—H_{Gln}	2.55	2.11	2.19	2.22
H1—O(wat)		2.78	2.63	
N1—Ru—S1	169.5	174.0	171.4	171.5
N_{his}—Ru—NO		101.1	96.4	97.5
NO—Ru—Cl3		65.6	88.3	87.2
Cl3—Ru—Cl4	94.8	101.2	89.0	88.8
Cl4—Ru—N_{his}	86.9	91.6	86.2	86.5
N_{his}—Ru—O(wat)	100.1			
O(wat)—Ru—Cl3	78.1			

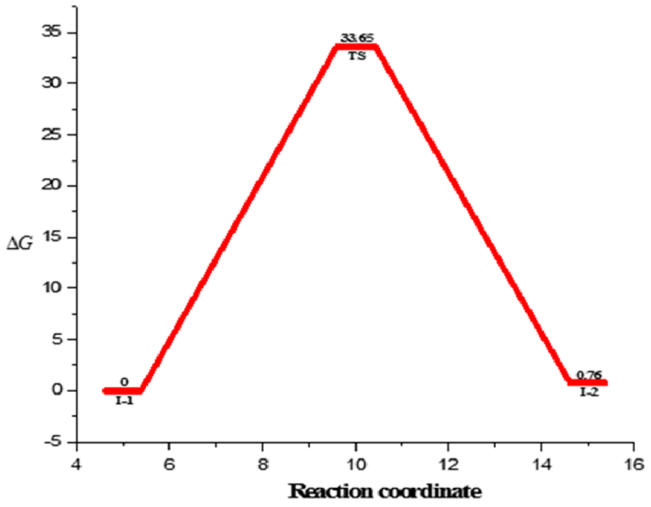

Figure 3. Free energy profile diagram of the hydrolysis step of NAMI-A-HSA adduct in gas phase calculated at the B3LYP/(LanL2DZ+6-31G(d,p)) level.

Table 3. Total ZPE ($E_{tot/ZPE}$), Solvation Free Energies (G_{solv}), Thermal Contributions to Enthalpies (H_{therm}), Thermal Contribution to Gibbs Free Energies (G_{therm}), Change of Enthalpies (ΔH), and Change of Gibbs Free Energies (ΔG) at 298.15 K for the Species Involved in Hydrolysis Process of NAMI-A-HSA Adduct (Energy Values, kcal mol^{-1}; Entropy Values, cal k^{-1} mol^{-1}; Rate Constant Values, s^{-1}; Solvent Phase Values, in Parentheses)

species	$E_{tot/ZPE}$	G_{solv}	H_{therm}	G_{therm}	ΔH	ΔG	ΔS	k(gas)	k(solvent)
I-1	0	−33.87	355.67	264.26	0	0	0	1.35×10^{-12}	3.81×10^{-6}
TS	31.38	−42.67	355.55	266.65	31.26 (22.46)	33.65 (24.85)	−8.44		
I-2	−0.63	−38.28	354.97	265.75	−1.33 (−5.74)	0.76 (−3.65)	−7.36		

DOI: 10.1021/acs.jpcb.5b05071
J. Phys. Chem. B 2015, 119, 10456−10465

optimized intermediate structure of nitrosylation I-3, the hydrogen atom of the coordinated water molecule forms an interconnected hydrogen bonding interaction with the oxygen atom of the histidyl residue at 1.87 Å. In I-3, the bond distance between the nitrogen atom of NO molecule with ruthenium ion is 3.89 Å. Transition state TS1, a heptacoordinate geometry, is confirmed by the presence of one imaginary frequency. In TS1, the entering NO molecule approaches the reaction center where the Ru—NO distance decreases from 3.89 to 3.80 Å, while, the leaving water ligand moves from the reaction center with the Ru—O distance increasing from 2.25 to 5.96 Å, indicating a dissociative character of the transition state. In the I-4 intermediate structure, the incoming NO group (Ru—NO = 1.78 Å) replaces the water ligand (Ru—H_2O = 5.01 Å) and coordinates with the ruthenium center. Thus, the nitrosylation product P1 has a pseudo-octahedral geometry, where water ligand is completely removed from the system by NO. NO strongly binds in the adduct P1, resulting in the reduction of the Ru^{3+} to Ru^{2+} ion to form a linear Ru^{2+}—NO^+ bond.

Ru^{3+} ion associated with d^5 electronic configuration becomes more stable than that of Ru^{2+} ion due to symmetrical distribution of electronic charge and more exchange energy. NO, when coordinated with Ru^{3+}, transfers its unpaired electron to the ruthenium ion, making the spin coupled linear Ru^{2+}—NO^+ adduct P1, in agreement with experimental studies by Oszajca et al.[15] The reduction potential for P1 is observed to be −2.32 V, which is closer to the experimental reduction potential value.[15] Ru^{2+} ion with d^6 electronic configuration exhibits lesser stability than Ru^{3+} since distribution of electronic charge is not uniform and exchange energy of electrons is less and, hence, more reactive. Thus, NO interaction plays an important role in describing the antimetastatic activity of NAMI-A. The probable mode of action involved in the NO interaction to NAMI-A-HSA is as follows:[57]

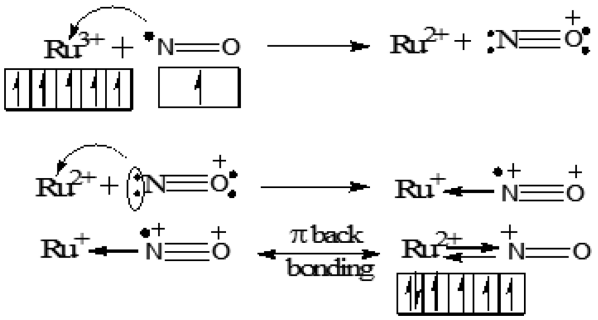

Energy Profiles. *Hydrolysis.* The change of enthalpies, Gibbs free energies, solvation energies, thermal corrections to the enthalpies, and thermal contribution to the Gibbs free energies of the stationary points for the hydrolysis reaction of NAMI-A-HSA adduct at 298.15 K in the gas and solvent phases calculated at DFT-B3LYP level are presented in Table 3. On the basis of these results, relative Gibbs free energies corresponding to the hydrolysis process of NAMI-A-HSA adduct computed in the gas and solvent phases are provided in the form of a reaction profile diagram in Figures 3 and 4. It can be noted from Figure 3 that the activation free energy for the hydrolysis of NAMI-A-HSA adduct is found to be 33.65 kcal mol^{-1}. Incorporation of solvent (water) effect by using the CPCM model lowers the activation free energy for this hydrolysis reaction and is found to be 24.85 kcal mol^{-1}, which is in agreement with the experimental activation energy value reported by Bouma et al.[58] The decrease in activation free energy in aqueous medium may be due to the fact that, in aqueous medium, all of the reactants, intermediates,

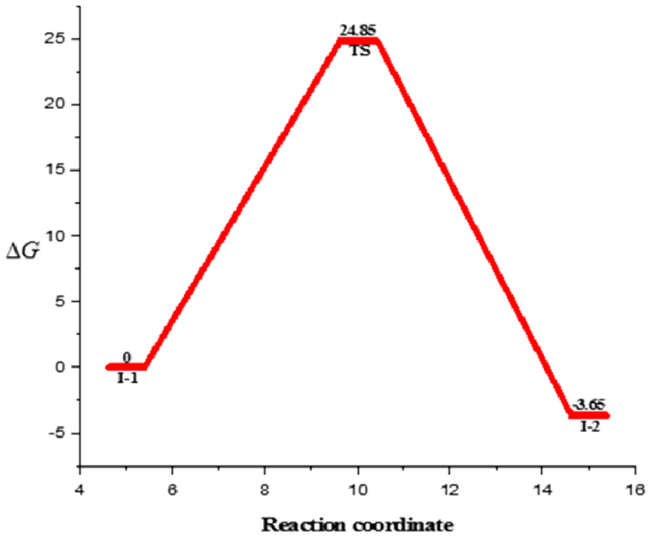

Figure 4. Free energy profile diagram of the hydrolysis step of NAMI-A-HSA adduct in solvent phase calculated at the B3LYP/(LanL2DZ+6-31G(d,p)) level.

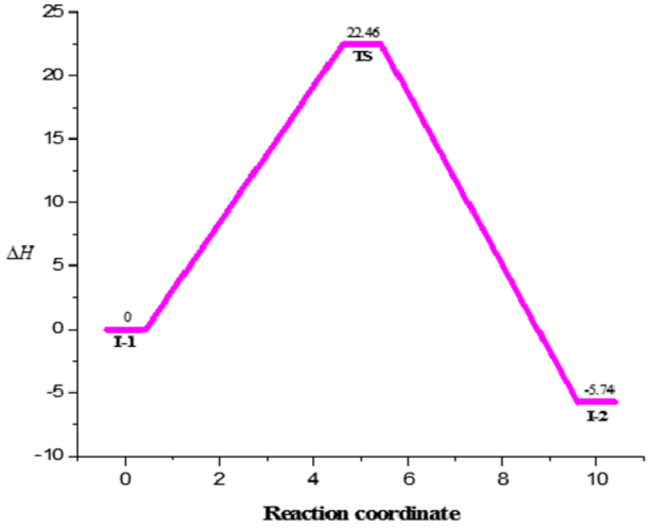

Figure 5. Enthalpy profile diagram of the hydrolysis step of NAMI-A-HSA adduct in solvent phase calculated at the B3LYP/(LanL2DZ+6-31G(d,p)) level.

and product species remain in the solvation state. Solvation lowers the energy of the species and makes the reaction easier. In Figure 5 we have presented the computed enthalpy profile for the hydrolysis reaction of NAMI-A-HSA adduct in the solvent phase. It has been observed that activation enthalpy for the hydrolysis reaction in solvent phase is 22.46 kcal mol^{-1} in agreement with the experimental evidence.[58] Moreover, the hydrolysis reaction is predicted to be exothermic by 5.74 kcal mol^{-1} in the solvent phase, as observed from Figure 5 indicating that the reaction is thermodynamically favored.

Nitrosylation. The change of enthalpies, Gibbs free energies, solvation energies, thermal corrections to the enthalpies, and thermal contribution to Gibbs free energies at 298.15 K of all of the stationary points of the nitrosylation reaction of hydrolyzed NAMI-A-HSA adduct in gas as well as solvent phases are presented in Table 4. The Gibbs free energy diagrams for the water exchange reaction of hydrolyzed NAMI-A-HSA adduct with NO in the gas and solvent phases are shown in

DOI: 10.1021/acs.jpcb.5b05071
J. Phys. Chem. B 2015, 119, 10456−10465

Table 4. Total ZPE ($E_{tot/ZPE}$), Solvation Free Energies (G_{solv}), Thermal Contributions to Enthalpies (H_{therm}), Thermal Contribution to Gibbs Free Energies (G_{therm}), Change of Enthalpies (ΔH), Change of Gibbs Free Energies (ΔG), and Rate Constant at 298.15 K for the Species Involved in the Nitrosylation Reaction of Hydrolyzed NAMI-A-HSA Adduct (Energy Values, kcal mol^{-1}; Entropy Values, cal k^{-1} mol^{-1}; Rate Constant Values, s^{-1}; Solvent Phase Values, in Parentheses)

species	$E_{tot/ZPE}$	G_{solv}	H_{therm}	G_{therm}	ΔH	ΔG	ΔS	k(gas)	k(solvent)
I-3	0	−66.52	357.77	269.75	0	0	0	2.57×10^{1}	2.99×10^{6}
TS1	22.59	−73.42	355.77	263.16	20.59 (13.69)	15.52 (8.62)	17.94		
I-4	−38.27	−67.77	358.36	267.59	−37.78 (−38.93)	−40.40 (−41.55)	8.84		

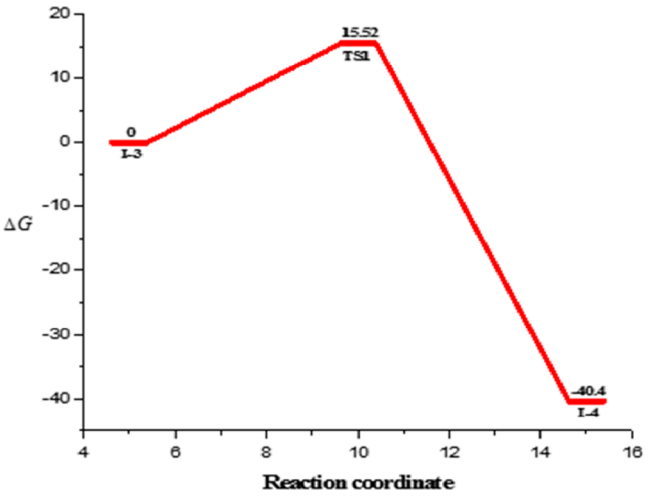

Figure 6. Free energy profile diagram of the nitrosylation step of NAMI-A-HSA adduct in gas phase calculated at the B3LYP/(LanL2DZ+6-31G(d,p)) level.

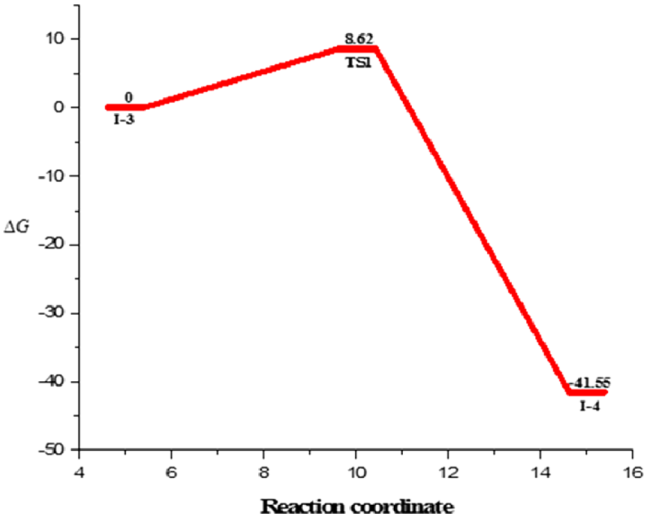

Figure 7. Free energy profile diagram of the nitrosylation step of NAMI-A-HSA adduct in solvent phase calculated at the B3LYP/(LanL2DZ+6-31G(d,p)) level.

Figures 6 and 7. Comparing the energy diagrams of Figures 6 and 7, it is noticed that inclusion of solvent effect reduces the activation free energy from 15.52 to 8.62 kcal mol^{-1}. The decrease in activation energy in aqueous medium is due to solvation which solvates the reactant and intermediate species through a hydrogen bonding network. The hydrogen bonding network stabilized the solvated species to a greater extent by decreasing its energy, hence, enhancing the stability of the activated complex and making the nitrosylation reaction more feasible in aqueous medium than in gas medium. Figure 8

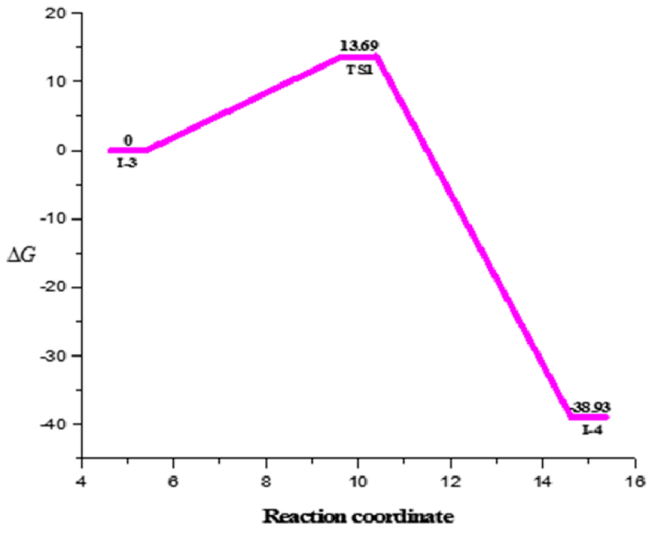

Figure 8. Enthalpy profile diagram of the nitrosylation step of NAMI-A-HSA adduct in solvent phase calculated at the B3LYP/(LanL2DZ+6-31G(d,p)) level.

displays the enthalpy profile diagram for the water exchange reaction of hydrolyzed NAMI-A-HSA adduct with nitric oxide in solvent medium. The activation enthalpy value for this nitrosylation reaction is observed to be 13.69 kcal mol^{-1}, and the reaction is exothermic by 38.93 kcal mol^{-1}.

Kinetic Analysis. The rate constant values for aquation and nitrosylation reaction of NAMI-A-HSA adduct are calculated by using the Eyring equation via activation free energy values, and results are summarized in Table 3 (hydrolysis reaction) and Table 4 (nitrosylation reaction). The calculated rate constant for the hydrolysis of NAMI-A-HSA adduct in aqueous solution ($k = 3.81 \times 10^{-6}$ s^{-1}) is found to be closer to the experimental values of Cl$^-$ hydrolysis of NAMI-A reported by Bouma et al. (5.58×10^{-6} s^{-1} in phosphate buffer (pH 7.4) when exposed to light).[59] A higher rate constant value in the solvent phase compared to the gas phase ($k = 1.35 \times 10^{-12}$ s^{-1}) shows the importance of solvent effect on the hydrolysis reaction of the NAMI-A-HSA adduct. The rate constant value for the water exchange reaction of NAMI-A-HSA adduct with nitric oxide is observed to be $k = 2.99 \times 10^{6}$ s^{-1} in aqueous phase while the gas phase value is $k = 2.57 \times 10^{1}$ s^{-1}, revealing that the rate of nitrosylation reaction is much faster in the aqueous phase. The rate constant values for NO binding to hydrolyzed NAMI-A-HSA adduct in solvent medium can be comparable with available literature of NO binding to ferric iron in micro-peroxidase.[60]

Relative Free Energy of Binding ($\Delta\Delta G$). The relative solvation free energy ($\Delta\Delta G_{solv}$) and binding free energy ($\Delta\Delta G_{bind}$) calculated using the thermodynamic cycle perturbation (Scheme1) are reported in Table 5. $\Delta\Delta G_{solv}$ are evaluated by mutating a water molecule to the NAMI-A-HSA adduct

DOI: 10.1021/acs.jpcb.5b05071
J. Phys. Chem. B 2015, 119, 10456−10465

Table 5. Relative Solvation Energy ($\Delta\Delta G_{solv}$) and Relative Free Energy of Binding ($\Delta\Delta G_{bind}$) for Hydrolysis and Nitrosylation of NAMI-A-HSA Adduct (Binding Energy Values, kcal mol^{-1})

	$\Delta\Delta G_{solv}$		$\Delta\Delta G_{bind}$	
species	$\Delta G_2 - \Delta G_1$	$\Delta G_{aq} - \Delta G_{gas}$	$\Delta G_4 - \Delta G_3$	$\Delta G_{adduct} - \Delta G_{aq}$
NAMI-A-HSA → NAMI-A-HSA-H_2O	−16.94	−16.94	−525.23	−525.23
NAMI-A-HSA-H_2O → NAMI-A-HSA-NO	−44.55	−44.55	−176.96	−176.96

(a)

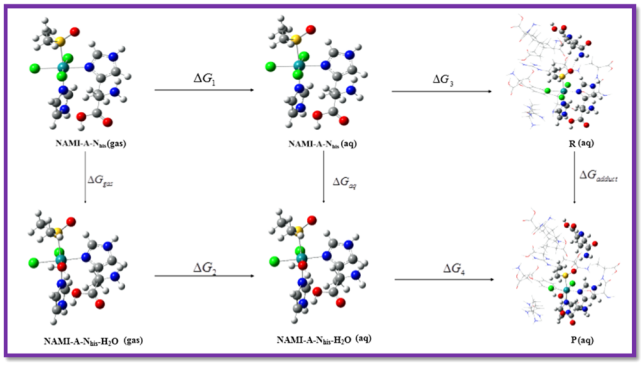

(b)

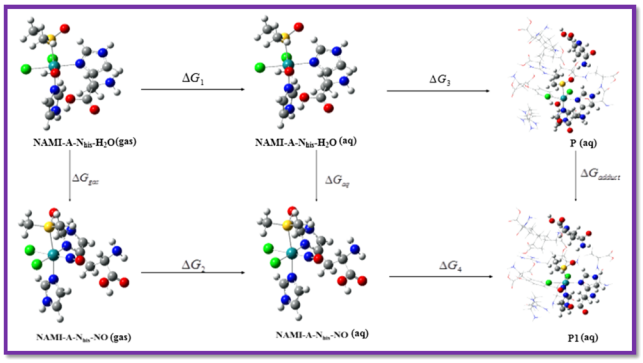

Figure 9. Thermodynamic cycle for (a) hydrolysis and (b) nitrosylation reaction.

(QM part) and nitric oxide to the hydrolyzed NAMI-A-HSA adduct (QM part) in water and gas phases. For relative $\Delta\Delta G_{bind}$ calculation, simulations are carried out by mutating a water molecule to the NAMI-A-HSA adduct and NO to the hydrolyzed NAMI-A-HSA adduct both in the water and in the protein (Figure 9). The calculated solvation relative free energy $\Delta\Delta G_{solv}$ defined as $\Delta G_{aq} - \Delta G_{gas}$ is found to be equal to $\Delta G_2 - \Delta G_1$, indicating that $\Delta\Delta G_{solv}$ follows a closed thermodynamic cycle. Similarly $\Delta\Delta G_{bind}$ also follows a closed thermodynamic cycle. The calculated relative $\Delta\Delta G_{bind}$ values for the mutations of water to the NAMI-A-HSA adduct and nitric oxide to the hydrolyzed NAMI-A-HSA adduct are −525.23 and −176.96 kcal mol^{-1}, respectively (Table 5). Thus, it can be seen that the relative binding free energies for the mutation of the water molecule to NAMI-A-HSA adduct and mutation of nitric oxide molecule to hydrolyzed NAMI-HSA adduct are negative, suggesting that the hydrolysis and nitrosylation reaction of NAMI-A-HSA adduct is favorable. Again, in order to predict $\Delta\Delta G_{bind}$ more accurately, the thermodynamic perturbation method must predict accurately the relative solvation free energies of the ligands. The calculated relative $\Delta\Delta G_{solv}$) are found to be negative (Table 5) which revealed that all of the reactant species are better solvated in the water medium and, hence, reaction occurs more easily in solvent medium.

CONCLUSION

In the present study, we have computationally investigated the hydrolysis mechanism of NAMI-A-HSA adduct using the DFT-B3LYP method. Hence, nitrosylation of hydrolyzed NAMI-A-HSA adduct with nitric oxide is also performed in order to understand the antimetastatic property of NAMI-A. Our computed results reveal that the mechanism responsible for chloride exchange reaction in NAMI-A-HSA adducts with water is an interchange dissociative mechanism, passing through a heptacoordinate transition state. Activation free energy and rate constant values for this reaction are found to be 24.85 kcal mol^{-1} and 3.81 × 10^{-6} s^{-1} in the solvent phase, in agreement with experimental values. The transition state of the ligand exchange reaction of the hydrolyzed form of NAMI-A-HSA adduct with nitric oxide is found to be of heptacoordinated geometry. Similar to hydrolysis of NAMI-A-HSA adduct, nitrosylation also leads to a lower activation free energy value in solvent medium (8.62 kcal mol^{-1}) than the gas medium (15.52 kcal mol^{-1}). The rate constant value for nitrosylation in the solvent medium is 2.99 × 10^{6} s^{-1}, correlate experimental results and concern reaction is also found to be exothermic. These results reveal that the nitric oxide exchange reaction is fast and favorable. It is interesting to note that nitric oxide reduces ruthenium(III) to active ruthenium(II) with a reduction potential of −2.32 V. Calculated relative free energies of binding ($\Delta\Delta G_{bind}$) obtained for hydrolysis and nitrosylation reaction of NAMI-A-HSA adduct show a close thermodynamic cycle. The negative relative $\Delta\Delta G_{bind}$ for mutation of water to NAMI-A-HSA adduct to form hydrolyzed NAMI-A-HSA adduct and mutation of NO to hydrolyzed NAMI-A-HSA adduct to form nitrosylyzed NAMI-A-HSA adduct show that hydrolysis and nitrosylation reactions are favorable. Our present work provides detailed structural properties and energy profiles for the hydrolysis and nitrosylation mechanism of NAMI-A, inside the protein environment which may contribute to the understanding of the antimetastatic activity of this drug as well as its NO scavenging ability.

ASSOCIATED CONTENT

Supporting Information

Cartesian coordinates for the transition state involved in the hydrolysis process of NAMI-A-HSA adduct and *XYZ* coordinates of all optimized structures. The Supporting Information is available free of charge on the ACS Publications website at DOI: 10.1021/acs.jpcb.5b05071.

AUTHOR INFORMATION

Corresponding Author

*E-mail: paritos_au@yahoo.co.in.

Notes

The authors declare no competing financial interest.

ACKNOWLEDGMENTS

P.M. thanks the Department of Science and Technology (DST, New Delhi, India) for financial support (Grant SERB/F/1672/

DOI: 10.1021/acs.jpcb.5b05071
J. Phys. Chem. B 2015, 119, 10456−10465

2013-14). D.D. is thankful to the University Grants Commission (UGC), New Delhi for providing a research fellowship.

REFERENCES

(1) Bergamo, A.; Gaiddon, C.; Schellens, J. H. M.; Beijnen, J. H.; Sava, G. Approaching Tumour Therapy Beyond Platinum Drugs Status of the Art and Perspectives of Ruthenium Drug Candidates. *J. Inorg. Biochem.* **2012**, *106*, 90−99.

(2) Antonarakis, E. S.; Ashkan, E. Ruthenium-Based Chemotherapeutics: Are They Ready for Prime Time? *Cancer Chemother. Pharmacol.* **2010**, *66*, 1−9.

(3) Clarke, M. J.; Zhu, F.; Frasca, D. R. *Chem. Rev.* **1999**, *99*, 2511−2534.

(4) Allardyce, C. S.; Dyson, P. J. Ruthenium in Medicine: Current Clinical uses and Future Prospects. *Platinum Met. Rev.* **2001**, *45*, 62−69.

(5) Dwyer, F. P.; Gyarfas, E. C.; Rogers, W. P.; Koch, J. H. Biological Activity of Complex Ions. *Nature* **1952**, *170*, 190−191.

(6) Clarke, M. J. *Oncological Implications of the Chemistry of Ruthenium*. In *Metal Ions in Biological Systems*; Sigel, H., Ed.; Marcel Dekker: New York, 1980. p 231−283.

(7) Hartinger, C. G.; Jakupec, M. A.; Zorbas-Seifried, S.; Groessl, M.; Egger, A.; Berger, W.; Zorbas, H.; Dyson, P. J.; Keppler, B. K. KP1019, A New Redox-Active Anticancer Agent − Preclinical Development and Results of a Clinical Phase I Study in Tumor Patients. *Chem. Biodiversity* **2008**, *5*, 2140−2155.

(8) Levina, A.; Mitra, A.; Lay, P. A. Recent Developments in Ruthenium Anticancer Drugs. *Metallomics* **2009**, *1*, 458−470.

(9) Sanchez-Cano, C.; Hannon, M. J. Novel and Emerging Approaches for the Delivery of Metallo-Drug. *Dalton Trans.* **2009**, *48*, 10702−10711.

(10) Gava, B.; Zorzet, S.; Spessotto, P.; Cocchietto, M.; Sava, G. Inhibition of B16 Melanoma Metastases with the Ruthenium Complex Imidazolium *trans*-Imidazoledimethylsulfoxidetetrachlororuthenate and Down-Regulation of Tumor Cell Invasion. *J. Pharmacol. Exp. Ther.* **2006**, *317*, 284−291.

(11) Zorzet, S.; Sorc, A.; Casarsa, C.; Cocchietto, M.; Sava, G. Pharmacological Effects of the Ruthenium Complex NAMI-A Given Orally to CBA Mice with MCa Mammary Carcinoma. *Met.-Based Drugs* **2001**, *8*, 1−7.

(12) Sava, G.; Capozzi, I.; Clerici, K.; Gagliardi, G.; Alessio, E.; Mestroni, G. Pharmacological Control of Lung Metastases of Solid Tumours by a Novel Ruthenium Complex. *Clin. Exp. Metastasis* **1998**, *16*, 371−379.

(13) Ang, W. H.; Dyson, P. J. Classical and Non-Classical Ruthenium-Based Anticancer Drugs: Towards Targeted Chemotherapy. *Eur. J. Inorg. Chem.* **2006**, *20*, 4003−4018.

(14) Zorzet, S.; Bergamo, A.; Cocchietto, M.; Sorc, A.; Gava, B. Lack of *In Vitro* Cytotoxicity, Associated to Increased G2-M Cell Fraction and Inhibition of Matrigel Invasion, May Predict *In Vivo*-Selective Antimetastasis Activity of Ruthenium Complexes. *J. Pharmacol. Exp. Ther.* **2000**, *295*, 927−933.

(15) Oszajca, M.; Kulis, E.; Stochel, G.; Brindell, M. Interaction of the NAMI-A Complex with Nitric oxide Under Physiological Conditions. *New J. Chem.* **2014**, *38*, 3386−3394.

(16) Brindell, M.; Stawoska, I.; Supel, J.; Skoczowski, A.; Stochel, G.; van Eldik, R. The Reduction of (ImH)[*trans*-RuIIICl_4(dmso)(Im)] Under Physiological Conditions: Preferential Reaction of the Reduced Complex with Human Serum Albumin. *JBIC, J. Biol. Inorg. Chem.* **2008**, *13*, 909−918.

(17) Vargiu, A. V.; Robertazzi, A.; Magistrato, A.; Ruggerone, P.; Carloni, P. The Hydrolysis Mechanism of the Anticancer Ruthenium Drugs NAMI-A and ICR Investigated by DFT−PCM Calculations. *J. Phys. Chem. B* **2008**, *112*, 4401−4409.

(18) Schluga, P.; Hartinger, C. G.; Egger, A.; Reisner, E.; Galanski, M.; Jakupec, M. A.; Keppler, B. K. Redox Behavior of Tumor-Inhibiting Ruthenium(III) Complexes and Effects of Physiological Reductants on their Binding to GMP. *Dalton Trans.* **2006**, *14*, 1796−1802.

(19) Clarke, M. J. Ruthenium Metallophamaceuticals. *Coord. Chem. Rev.* **2002**, *232*, 69−93.

(20) Qian, Z. M.; Li, H.; Sun, H.; Ho, K. Targeted Drug Delivery via the Transferrin Receptor-Mediated Endocytosis Pathway. *Pharmacol Rev.* **2002**, *54*, 561−587.

(21) Crichton, R.; Charloteaux-Wauters, R. Iron Transport and Storage. *Eur. J. Biochem.* **1987**, *164*, 485−506.

(22) Serli, B.; Zangrando, E.; Gianferrara, T.; Yellowlees, L.; Alessio, E. Coordination and Release of NO by Ruthenium-Dimethylsulfoxide Complexes-Implications for Anti-Metastases Activity. *Coord. Chem. Rev.* **2003**, *245*, 73−83.

(23) Morbidelli, L.; Donnini, S.; Filippi, S.; Messori, L.; Piccioli, F.; Orioli, P.; Sava, G.; Ziche, M. Antiangiogenic Properties of Selected Ruthenium(III) Complexes That Are Nitric Oxide Scavengers. *Br. J. Cancer* **2003**, *88*, 1484−1491.

(24) Tfouni, E.; Truzzi, D. R.; Tavares, A.; Gomes, A. J.; Figueiredo, L. E.; Franco, D. W. Biological Activity of Ruthenium Nitrosyl Complexes. *Nitric Oxide* **2012**, *26*, 38−53.

(25) Silverman, R. B. Design of Selective Neuronal Nitric Oxide Synthase Inhibitors for the Prevention and Treatment of Neurodegenerative Diseases. *Acc. Chem. Res.* **2009**, *42*, 439−451.

(26) Hou, Y. C.; Janczuk, A.; Wang, P. G. Current Trends in the Development of Nitric Oxide Donors. *Curr. Pharm. Des.* **1999**, *5*, 417−441.

(27) Fukumura, D.; Yuan, F.; Endo, M.; Jain, R. K. Role of Nitric oxide in Tumor Microcirculation. Blood flow, Vascular Permeability, and Leukocyte-Endothelial Interactions. *Am. J. Pathol.* **1997**, *150*, 713−725.

(28) Wink, D. A.; Vodovotz, Y.; Laval, J.; Lava, F.; Dewhirst, M. W.; Mitchell, J. B. The Multifaceted Roles of Nitric Oxide in Cancer. *Cancerogenesis* **1998**, *19*, 711−721.

(29) Gallo, O.; Masini, E.; Morbidelli, L.; Franchi, A.; Fini-Storchi, I.; Vergari, W. A.; Ziche, M. Angiogenesis and Tumor Progression are Under the Control of Nitric Oxide in Head and Neck Cancer. *J. Natl. Cancer Inst.* **1998**, *90*, 587−596.

(30) Klotz, T.; Bloch, W.; Volberg, C.; Engelmann, U.; Addicks, K. Selective Expression of Inducible Nitric Oxide Synthase in Human Prostate Carcinoma. *Cancer* **1998**, *82*, 1897−1903.

(31) Jadeski, L. C.; Hum, K. O.; Chakraborty, C.; Lala, P. K. Nitric Oxide Promotes Murine Mammary Tumour Growth and Metastasis by Stimulating Tumour Cell Migration, Invasiveness and Angiogenesis. *Int. J. Cancer* **2000**, *86*, 30−39.

(32) Jadeski, L. C.; Lala, P. K. Nitric Oxide Synthase Inhibition By N(G)-Nitro-L-Arginine Methyl Ester Inhibits Tumor-Induced Angiogenesis in Mammary Tumors. *Am. J. Pathol.* **1999**, *155*, 1381−1390.

(33) Swaroop, G. R.; Kelly, P. A.; Bell, H. S.; Shinoda, J.; Yamaguchi, S.; Whittle, I. R. The Effects of Chronic Nitric Oxide Synthase Suppression on Glioma Pathophysiology. *Br. J. Neurosurg.* **2000**, *14*, 543−548.

(34) Sanna, B.; Debidda, M.; Pintus, G.; Tadolini, B.; Posadino, A. M.; Bennardini, F.; Sava, G.; Ventura, C. The Anti-Metastatic Agent Imidazolium *trans*-Imidazoledimethylsulfoxide-Tetrachlororuthenate Induces Endothelial Cell Apoptosis by Inhibiting The Mitogen-Activated Protein Kinase/Extracellular Signal-Regulated Kinase Signaling Pathway. *Arch. Biochem. Biophys.* **2002**, *403*, 209−218.

(35) Vacca, A.; Bruno, M.; Boccarelli, A.; Coluccia, M.; Ribatti, D.; Bergamo, A.; Garbisa, S.; Sartor, L.; Sava, G. Inhibition of Endothelial Cell Functions and of Angiogenesis by the Metastasis Inhibitor NAMI-A. *Br. J. Cancer* **2002**, *86*, 993−998.

(36) Hartinger, C. G.; Zorbas-Seifried, S.; Jakupec, M. A.; Kynast, B.; Zorbas, B. H.; Keppler, B. K. From Bench to Bedside–Preclinical and Early Clinical Development of the Anticancer Agent Indazolium *trans*-[Tetrachlorobis(1*H*-indazole)ruthenate(III)] (KP1019 or FFC14A). *J. Inorg. Biochem.* **2006**, *100*, 891−904.

(37) Bytzek, A. K.; Boeck, K.; Hermann, G.; Hann, S.; Keppler, B. K.; Hartinger, C. G.; Koellensperger, G. LC- and CZE-ICP-MS Approaches for the *in vivo* Analysis of the Anticancer Drug Candidate Sodium *trans*-[Tetrachloridobis(1*H*-indazole)ruthenate(III)] (KP1339) in Mouse Plasma. *Metallomics* **2011**, *3*, 1049−1055.

(38) Storr, T.; Cameron, B. R.; Gossage, R. A.; Yee, H.; Skerlj, R. T.; Darkes, M. C.; Fricker, S. P.; Bridger, G. J.; Davies, N. A.; Wilson, M. T.; et al. Ru^{III} complexes of Edta and Dtpa Polyaminocarboxylate Analogues

DOI: 10.1021/acs.jpcb.5b05071
J. Phys. Chem. B 2015, 119, 10456−10465

and Their Use in Nitric Oxide Scavengers. *Eur. J. Inorg. Chem.* **2005**, *2005*, 2685−2697.
(39) Storr, T.; Cameron, B. R.; Gossage, R. A.; Yee, H.; Skerlj, R. T.; Darkes, M. C.; Fricker, S. P.; Bridger, G. J.; Davies, N. A.; Wilson, M. T.; et al. Ru^{III} Complexes of Edta and Dtpa Polyaminocarboxylate Analogues and Their Use as Nitric Oxide Scavengers. *Eur. J. Inorg. Chem.* **2005**, *2005*, 2685−2697.
(40) Serli, B.; Zangrando, E.; Iengo, E.; Mestroni, G.; Yellowlees, L.; Alessio, E. Synthesis and Structural, Spectroscopic, and Electrochemical Characterization of New Ruthenium Dimethyl Sulfoxide Nitrosyls. *Inorg. Chem.* **2002**, *41*, 4033−4043.
(41) Cameron, B. R.; Darkes, M. C.; Yee, H.; Olsen, M.; Fricker, S. P.; Skerlj, R. T.; Bridger, G. J.; Davies, N. A.; Wilson, M. T.; Rose, D. J.; et al. Ruthenium(III) Polyaminocarboxylate Complexes: Efficient and Effective Nitric Oxide Scavengers. *Inorg. Chem.* **2003**, *42*, 1868−1876.
(42) Mosi, R.; Seguin, B.; Cameron, B.; Amankwa, L.; Darkes, M. C.; Fricker, S. P. Mechanistic Studies on AMD6221: a Ruthenium-Based Nitric Oxide Scavenger. *Biochem. Biophys. Res. Commun.* **2002**, *292*, 519−529.
(43) Das, D.; Dutta, A.; Mondal, P. Interactions of the Aquated forms of Ruthenium(III) Anticancer Drugs with Protein: A Detailed Molecular Docking and QM/MM Investigation. *RSC Adv.* **2014**, *4*, 60548−60556.
(44) Frisch, M. J.; Trucks, G. W.; Schlegel, H. B.; Scuseria, G. E.; Robb, M. A.; Cheeseman, J. R.; Scalmani, G.; Barone, V.; Mennucci, B.; Petersson, G. A.; et al. *Gaussian 09*, Revision B.01; Gaussian: Wallingford, CT, USA, 2010.
(45) Lee, C.; Yang, W.; Parr, R. G. Development of the Colle-Salvetti Correlation-Energy Formula into a Functional of the Electron Density. *Phys. Rev. B: Condens. Matter Mater. Phys.* **1988**, *37*, 785−789.
(46) Hay, P. J.; Wadt, W. R. Ab Initio Effective Core Potentials for Molecular Calculations. Potentials for the Transition Metal Atoms Sc to Hg. *J. Chem. Phys.* **1985**, *82*, 270−284.
(47) Perdew, J. P.; Burke, K.; Wang, Y. Generalized Gradient Approximation for the Exchange-Correlation Hole of a Many-Electron System. *Phys. Rev. B: Condens. Matter Mater. Phys.* **1996**, *54*, 16533−16539.
(48) Gonzalez, C.; Schlegel, H. B. An Improved Algorithm for Reaction Path Following. *J. Chem. Phys.* **1989**, *90*, 2154−2161.
(49) Gonzalez, C.; Schlegel, H. B. Reaction Path Following in Mass-Weighted Internal Coordinates. *J. Phys. Chem.* **1990**, *94*, 5523−5527.
(50) Deubel, D. V.; Lau, J. K.-C. In Silico Evolution of Substrate Selectivity: Comparison of Organometallic Ruthenium Complexes with the Anticancer Drug Cisplatin. *Chem. Commun.* **2006**, 2451−2453.
(51) Lau, J. K. C.; Deubel, D. V. Hydrolysis of the Anticancer Drug Cisplatin: Pitfalls in the Interpretation of Quantum Chemical Calculations. *J. Chem. Theory Comput.* **2006**, *2*, 103−106.
(52) Barone, V.; Cossi, M. Quantum Calculation of Molecular Energies and Energy Gradients in Solution by a Conductor Solvent Model. *J. Phys. Chem. A* **1998**, *102*, 1995−2001.
(53) Chen, J.; Chen, L.; Liao, S.; Siyan, L.; Zheng, K.; Ji, L. A Theoretical Study on the Hydrolysis Process of the Antimetastatic Ruthenium(III) Complex NAMI-A. *J. Phys. Chem. B* **2007**, *111*, 7862−7869.
(54) Connors, K. A. *Chemical Kinetics—The Study of Reaction Rates in Solution*; Wiley: New York, 1990; p 200.
(55) Tembre, B. L.; Mc Cammon, J. A. Ligand-Receptor Interactions. *Comput. Chem.* **1984**, *8*, 281−283.
(56) Alessio, E.; Balducci, G.; Lutman, A.; Mestroni, G.; Calligaris, M.; Attia, W. M. Synthesis and Characterization of two New Classes of Ruthenium(III)-Sulfoxide Complexes with Nitrogen Donor Ligands (L): Na[*trans*-$RuCl_4(R_2SO)(L)$] and *mer, cis*-RuCl3(R2SO)(R2SO)-(L). The Crystal Structure of Na[*trans*-$RuCl_4$(DMSO)(NH_3)] 2DMSO, Na[*trans*-$RuCl_4$(DMSO)(Im)] H_2O, Me_2CO (Im = imidazole) and *mer, cis*-$RuCl_3$(DMSO)(DMSO)(NH_3). *Inorg. Chim. Acta* **1993**, *203*, 205−217.
(57) Puri, B. R.; Sharma, L. R.; Kalia, K. C. *Principles of Inorganic Chemistry*; Vallabh: Delhi, India, 1966.
(58) Bouma, M.; Nuijen, B.; Jansen, M. T.; Sava, G.; Flaibani, A.; Bult, A.; Beijnen, J. H. A Kinetic Study of the Chemical Stability of the Antimetastatic Ruthenium Complex NAMI-A. *Int. J. Pharm.* **2002**, *248*, 239−246.
(59) Bouma, M.; Nuijen, B.; Jansen, M. T.; Sava, G.; Bult, A.; Beijnen, J. Photostability Profiles of the Experimental Antimetastatic Ruthenium Complex NAMI-A. *J. Pharm. Biomed. Anal.* **2002**, *30*, 1287−1296.
(60) Sharma, V. S.; Traylor, T. G.; Gardiner, R.; Mizukami, H. Reaction of Nitric Oxide with Heme Proteins and Model Compounds of Hemoglobin. *Biochemistry* **1987**, *26*, 3837−3843.

NOTE ADDED AFTER ASAP PUBLICATION

This paper was published ASAP on July 31, 2015. In the Results and Discussion, the graphic of the probable mode of action involved in the NO interaction to NAMI-A-HSA has been updated. The corrected version was reposted on August 5, 2015.

DOI: 10.1021/acs.jpcb.5b05071
J. Phys. Chem. B 2015, 119, 10456−10465